

Electron collision studies on the CH_2^+ molecular ion

K. Chakrabarti^{1,*}, J. Zs Mezei^{2,3,†}, I. F. Schneider^{3,‡} and J. Tennyson^{3,4§}

¹*Department of Mathematics, Scottish Church College, 700006 Kolkata, India*

²*HUN-REN Institute for Nuclear Research (ATOMKI), H-4001 Debrecen, Hungary*

³*LOMC-UMR6294, CNRS, Université Le Havre Normandie, 76600 Le Havre, France and*

⁴*Department of Physics and Astronomy, University College London, WC1E 6BT London, UK*

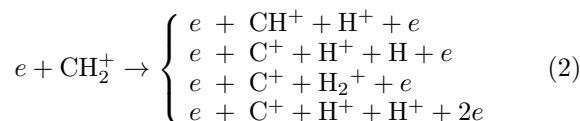
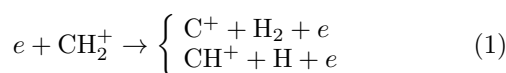
(Dated: May 22, 2024)

Calculations are performed for electron collision with the methylene molecular ion CH_2^+ in its bent equilibrium geometry, with the goal to obtain cross sections for electron impact excitation and dissociation. The polyatomic version of the UK molecular R-matrix codes was used to perform an initial configuration-interaction calculation on the doublet and quartet states of the CH_2^+ ion. Subsequently, scattering calculations are performed to obtain electron impact electronic excitation and dissociation cross sections and, additionally, the bound states of the CH_2 molecule and Feshbach resonances in the $e\text{-CH}_2^+$ system.

PACS numbers: 33.80. -b, 42.50. Hz

I. INTRODUCTION

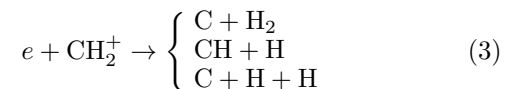
Many low temperature plasma environments have hydrocarbon molecular ions as important constituents. Collision of electrons with molecules and their ions in these environments are important processes that play a fundamental role in initiating chemistry, particle balance and transport. For example, although the present tendency in the magnetically controlled International Thermonuclear Fusion Reactor type fusion devices is to coat the reactor walls with beryllium or tungsten, hydrocarbon ions, in particular the methylene ion CH_2^+ , are found in the edge and divertor plasmas of fusion devices which operate with graphite as plasma facing material [1]. Another important context is that of the dusty plasmas, the CH_2 and CH_2^+ being species involved in the chain of reactions resulting in the growths of the nano and micro-particles. In these situations, the cross sections for different electron induced process are necessary to model the plasma flow (see for example [2]), in particular electron impact dissociation and dissociative ionisation:



These processes, leading to the destruction of the CH_2^+ ions and to the C atom production [3, 4], are highly significant for understanding the carbon redeposition.

In the interstellar medium (ISM), CH_2^+ ions are synthesised in gas phase by collision of C^+ ions with hydrogen

[5] and through hydrogen abstraction by CH^+ . On the other hand, CH_2^+ ions can be removed by reactions such as (1), (2) and by dissociative recombination (DR),



which is known to proceed via Feshbach resonances [6].

There is a considerable literature on CH_y^+ hydrocarbon ions, and CH_2^+ ions in particular, in the context of synthesis of hydrocarbons in the ISM [5, 7–10]. Significant work on CH_y^+ hydrocarbon ions have also been done relevant to plasmas for fusion [2–4, 11, 12]. These works mainly focus on different electron impact cross sections relevant for plasma modeling.

Molecular structure calculations on CH_2^+ have been reported by several authors [13–18]. [18] obtained bending potential energy curves (PEC) and vertical excitation energies of CH_2^+ for its bent C_{2v} and its linear $D_{\infty h}$ configurations. Accurate global potential energy surfaces (PES) were reported by [13] and [16]. Apart from these, there are also many spectroscopic studies on the rovibrational states of CH_2^+ [19–23].

In a number of earlier studies [24–27] we have studied electron collision with the CH molecule and its positive ion CH^+ in considerable detail. In these works, we not only computed cross sections for different electronic processes, but also identified many new neutral valence states of CH that are relevant for the DR. The present article aims to continue and extend our work to more complex hydrocarbon ions.

II. R-MATRIX CALCULATIONS

A. R-matrix method

The R-matrix method, described in detail by [28] and [29], and its implementation in the polyatomic version of the UK molecular R-matrix codes (UKRmol) [30] is used in the present work. The method employs a division of

*kkch@eth.net

†mezei.zsolt@atomki.hu

‡ioan.schneider@univ-lehavre.fr

§j.tennyson@ucl.ac.uk

space into an inner region, a sphere of radius a (chosen to be $10 a_0$ in this work) called the R -matrix sphere whose purpose is to include within it all short range interactions, and an outer region exterior to this sphere which contains all the long range interactions. This division allows the treatment of the short range and, the more complicated, long range interactions separately using different techniques [28].

In the inner region, the wave function of the target (here CH_2^+) and a single continuum electron, together having $N + 1$ electrons, is taken as

$$\Psi_k = \mathcal{A} \sum_{i,j} a_{i,j,k} \Phi_i(1, \dots, N) F_{i,j}(N+1) + \sum_i b_{i,k} \chi_i(1, \dots, N+1), \quad (4)$$

where \mathcal{A} is an antisymmetrisation operator, $\Phi_i(1, \dots, N)$ is the wave function of the N electron target and $F_{i,j}(N+1)$ are continuum orbitals. The functions $\chi_i(1, \dots, N+1)$ in the last term are square integrable functions, called L^2 functions, are constructed by allowing the projectile electron to enter the target complete active space (CAS) and are included to take into account electron correlations and polarization of the target in presence of the projectile electrons. The coefficients $a_{i,j,k}$ and $b_{i,k}$ are obtained by diagonalizing the inner region Hamiltonian.

The inner region wave function Ψ_k is then used with appropriate boundary conditions to obtain scattering information, the details of which are given in the following subsections.

B. Target calculations

We used the cc-pVTZ Gaussian basis sets [31] centered on the C and H atoms to represent the target orbitals. These not only gave reasonably good target vertical excitation energies but also allows the inner region calculation to remain manageable with respect to computational resources.

The X^2A_1 ground state of CH_2^+ is known to be bent in C_{2v} symmetry and has the electronic configuration $(1a_1)^2(2a_1)^2(1b_2)^2(3a_1)^1$ [32, 33]. In this work all calculations are reported at the equilibrium C-H bond length $2.066 a_0$ and the H-C-H bond angle 140.1° taken from [18], which are very close to those obtained by more sophisticated coupled cluster calculations using large basis sets [34]. An initial Hartree-Fock (HF) calculation was first performed on the X^2A_1 ground state of CH_2^+ . The HF orbitals were then used in a configuration interaction (CI) calculation.

We considered two target models. In both models we kept two electrons frozen in the $1a_1$ orbitals while the remaining five electrons were distributed in the CAS. In the first model (M1), the complete active space was defined by $(1a_1 - 6a_1, 1b_1 - 4b_1, 1b_2 - 4b_2)$, while in the second (M2) the CAS was chosen to be bigger with an additional $1a_2$ orbital, namely $(1a_1 - 8a_1, 1b_1 - 5b_1, 1b_2 - 5b_2, 1a_2)$. Table I shows the comparison of the vertical excitation

TABLE I: Comparison of the vertical excitation energies (in eV) from the X^2A_1 ground state to 12 low lying excited states of CH_2^+ for different target models. The target models used are the following:

M1: $(1a_1)^2(1a_1 - 6a_1, 1b_1 - 4b_1, 1b_2 - 4b_2)^5$

M2: $(1a_1)^2(1a_1 - 8a_1, 1b_1 - 5b_1, 1b_2 - 5b_2, 1a_2)^5$

Target state	M1	M2	Theory ^a	Theory ^b
X^2A_1	0 ^c	0 ^d	0 ^e	0
1^2B_1	0.92	0.81	0.84	0.83
1^4A_2	5.24	5.07		
1^2A_2	6.93	6.81	6.81	6.92
1^2B_2	7.46	7.36	7.60	7.8
2^2A_2	7.88	7.60	7.25	7.26
1^4B_1	9.73	9.58		
2^2B_2	9.48	9.17	9.25	9.6
2^2A_1	11.17	10.50	10.44	11.1
3^2A_1	13.52	13.04	12.81	
2^2B_1	13.47	13.21	13.14	13.9
4^2A_1	14.89	14.76	13.40	
3^2B_2	13.22	13.23	13.53	

^a[18]

^b[35]

^cAbsolute energy -38.61306904 Hartree

^dAbsolute energy -38.63754516 Hartree

^eAbsolute energy -38.705744 Hartree

energies (VEE) from the X^2A_1 ground state of CH_2^+ to the first 12 low lying excited states. Although the second model M2 appears to produce VEEs slightly in better agreement with the theoretical results of [18] and [35], calculations with this model required much longer time compared to the model M1. We therefore chose the model M1 for subsequent calculations as it was computationally more efficient.

From Table I, we see that apart from the VEE of the 4^2A_1 state, which appears too high compared to [18], all other vertical excitation energies obtained by the target model M1 are in reasonably good agreement with the results of [18] and [35]. Moreover, our dipole moment for the CH_2^+ ground state with model M1 is 0.701 D which compares perfectly with the value 0.701 D obtained by [34] using coupled cluster calculation. The model M1 therefore provides a good description of the target for subsequent scattering calculations.

C. Scattering calculations

For the scattering calculations, we used 8 a_1 , 6 b_1 , 6 b_2 and 2 a_2 target orbitals allowing 2 virtual orbitals for each symmetry. Since the target CH_2^+ is a positive ion, the continuum functions were represented by Coulomb functions which were obtained as a solution of the radial Coulomb equation for an isotropic Coulomb potential, and the solutions with $l \leq 4$, and energy eigenvalue ≤ 5 Ryd were retained in the calculation. The Coulomb functions were then fitted to GTOs using the procedure outlined in [36].

The target and continuum orbitals must all be orthogonal to each other. To ensure the orthogonality, the target

TABLE II: Comparison of the vertical excitation energies (in eV) from the ground X 3B_1 state of CH₂ to some of its low lying excited states.

CH ₂ state	This work	CI ^a	Romelt ^b	Yamaguchi ^c
X 3B_1	0.0 ^d	0.0 ^e	0.0 ^f	0.0
1 1A_1	1.16	0.995	1.14	
1B_1	1.74	1.86	1.63	
2 1A_1	3.24	3.31	3.38	
3A_1	6.21	7.67	6.37	
3B_2	7.35	8.05	7.59	7.86
1B_2	7.25	9.25	7.63	7.75
3A_2	7.63	7.47	7.57	7.23
1A_2	8.33	8.39	8.46	

^aCI calculation done at CH₂ equilibrium (C-H bond length 2.0314 a₀ and H-C-H bond angle 133.8°) using (1a₁)² (2a₁ - 6a₁, 1b₁ - 4b₁, 1b₂ - 4b₂)⁶ CAS-CI model.

^b[37]
^c[38]

^{d,e,f} Absolute energies of the ground states are respectively -38.985233^d Hartree, -38.966950^e Hartree and -39.06034^f Hartree.

and continuum orbitals were first individually Schmidt orthogonalized and finally the full set of target and continuum orbitals were symmetric orthogonalized, retaining only those orbitals for which the eigenvalue of their overlap matrix was less than a deletion threshold, chosen here to be 5×10^{-5} . The deletion threshold depends on the R-matrix radius and was adjusted to ensure that there was no linear dependence.

An R-matrix was built at the boundary of the inner and outer region from the inner region solutions (Eq.(4)). The R-matrix were then propagated to an asymptotic distance $R_{asy} = 70 a_0$ in a potential which included the Coulomb potential and the dipole and quadrupole potentials of the target, where they were then matched to asymptotic functions obtained from a Gailitis expansion [39]. This matching procedure yields the K-matrix from which all scattering observables can be obtained. A different route, however, is followed for obtaining bound states, as is outlined below.

For bound states, the R-matrix and wave functions were propagated using Runge- Kutta-Nystrom method [40] to an asymptotic distance $R_{asy} = 50 a_0$ in a potential which included the Coulomb potential and the dipole and quadrupole potentials of target, and were matched to exponentially decreasing asymptotic functions [39]. A searching algorithm [41] over a non-linear quantum defect based grid [42] was then used to find the bound states as roots of a determinant $B(E)$ dependent on the energy. The details of the method are omitted and can be found in [41].

III. RESULTS

All scattering calculations in this work were performed at a single geometry, namely the equilibrium geometry of the CH₂⁺ target ion, for bound states of the CH₂ molecule, Feshbach resonances in the e+CH₂⁺ system and

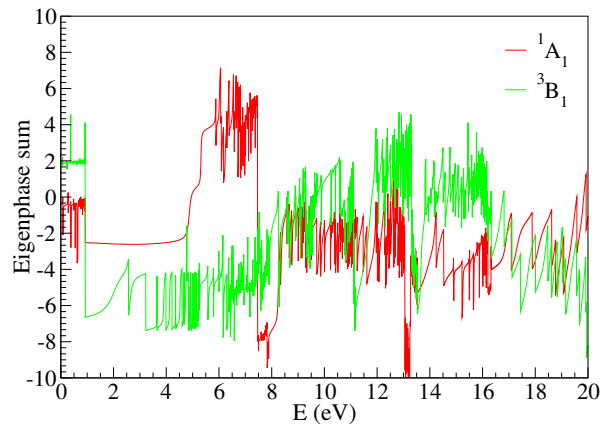


FIG. 1: Eigenphase sums for the overall e+ CH₂⁺ symmetries 1A_1 and 3B_1 .

cross sections for elastic scattering and electronic excitations. An 11 state scattering model including three 2A_1 , three 2B_1 , three 2B_1 and two 2A_2 target states in the close coupling expansion Eq. (4) were used for the singlet e+CH₂⁺ scattering close-coupling expansion, while a 15 state model which included the same 11 doublet states as in the singlet state model, together with the lowest each of the 4A_1 , 4B_1 , 4B_2 , and 4A_2 states was used in Eq. (4) for triplet symmetry close-coupling expansion. As will be shown below, this procedure provides a reliable scattering model which was tested by calculating the bound states of CH₂.

A. Bound states

Table II shows the vertical excitation energies for the bound states of CH₂ from its X 3B_1 ground state to few of its low lying excited states. For a comparison, we also did a quantum chemistry-style CI calculation on CH₂ at its equilibrium geometry (C-H bond length 2.0314 a₀ and H-C-H bond angle 133.8°) using a (1a₁)² (2 - 6a₁, 1 - 4b₁, 1 - 4b₂)⁶ CAS-CI model. The vertical excitation energies are then compared with the multi reference double excitation (MRD-CI) calculation of [37] and the coupled cluster results of [38]. From Table II, it is clear that the vertical excitation energies obtained by the R-matrix method are in very good agreement with all others. The fact that the calculated bound state energies are consistent and accurate enough indicates that our scattering model is reasonably good.

B. Resonances at equilibrium

For resonance calculation, the R-matrix was propagated to 70 a₀. Resonances were detected by the characteristic change in sign of the second derivative of the

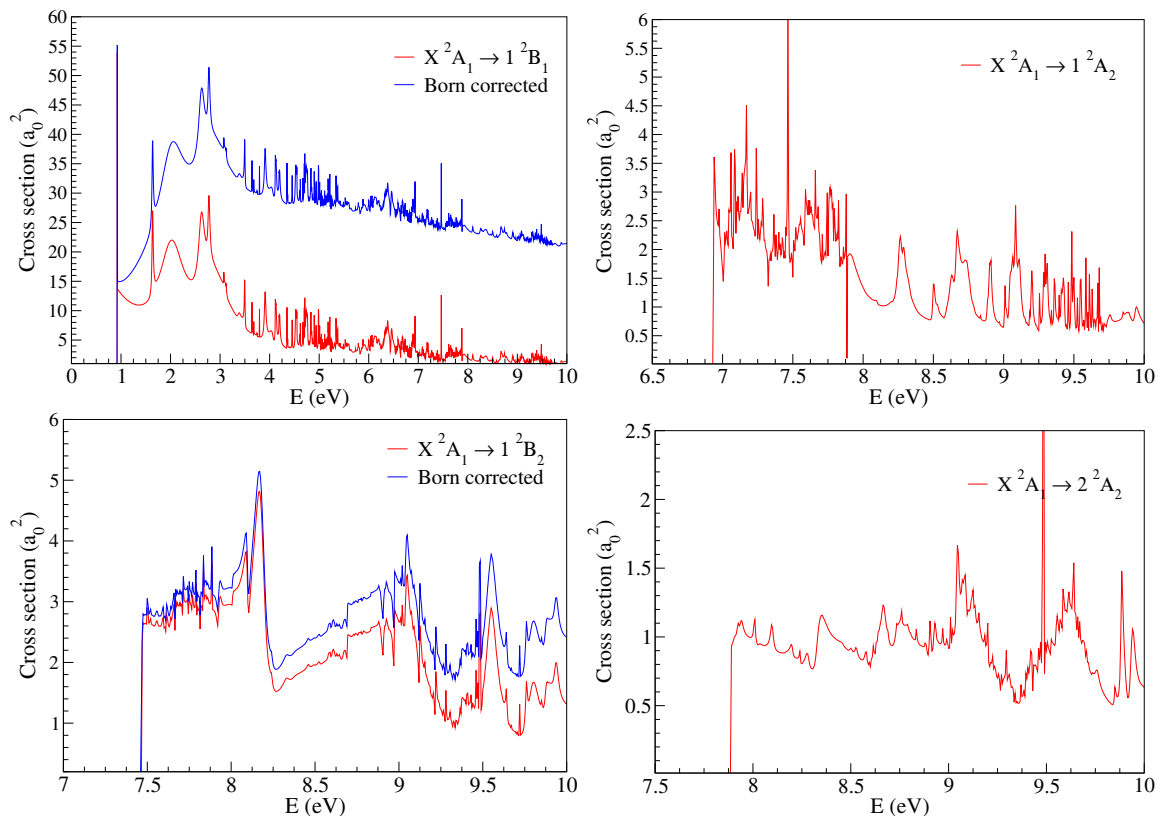


FIG. 2: Cross sections for electronic excitation from the X^2A_1 ground state to the first four excited states of doublet symmetry as given in Table I and indicated in each panel.

eigenphase sum $\delta(E)$ given by

$$\delta(E) = \sum_i \arctan(K_{ii}), \quad (5)$$

where K_{ii} are the diagonal elements of the K matrix. They were then fitted to a Breit-Wigner profile [43] with an energy grid 0.005 eV to obtain the resonance energy E and width Γ .

Figure 1 shows the plot of two typical eigenphase sums for 1A_1 and 3B_1 symmetries. Characteristic of electron collision with ions, the figure shows numerous resonances some of which are tabulated in Table III according to their parent state. As seen from the table, many of the resonances appear to be in Rydberg series which can be identified by their effective quantum numbers. The relatively small gap between the ground and first excited electronic state means that the resonances start with relatively high effective quantum numbers, $\nu \approx 4$, and then closely space.

A full set of fits to the resonances covering all overall scattering symmetries is given in the supplementary material.

TABLE III: Resonance positions and widths (in Ryd) and effective quantum numbers at the CH_2^+ equilibrium for states of 3B_1 and 1A_1 symmetry of the $e\text{-CH}_2^+$ system below the first two CH_2^+ excited states. Numbers within brackets indicate power of 10.

Position	Width	ν	Position	Width	ν
3B_1 symmetry					
Below 1^2B_1 state			Below 4^2A_2 state		
0.3558(-02)	0.2400(-04)	3.9466	0.1925	0.1075(-01)	2.2792
0.4870(-02)	0.5833(-04)	3.9875	0.2678	0.3334(-03)	2.9201
0.1567(-01)	0.4765(-04)	4.3815	0.2872	0.2789(-02)	3.1980
0.1718(-01)	0.6172(-04)	4.4465	0.3034	0.1910(-03)	3.5000
0.2685(-01)	0.1503(-04)	4.9440	0.3197	0.2426(-03)	3.9143
1A_1 symmetry					
Below 1^2B_1 state			Below 1^2A_2 state		
0.2034(-01)	0.2198(-03)	4.5925	0.3582	0.9116(-02)	2.5716
0.3582(-01)	0.1225(-03)	5.5953	0.3907	0.2355(-02)	2.9015
0.4478(-01)	0.7510(-04)	6.5969	0.4323	0.1280(-02)	3.6009
0.5043(-01)	0.4929(-04)	7.5979	0.4424	0.2339(-02)	3.8615
0.5423(-01)	0.3407(-04)	8.5985	0.4492	0.3074(-02)	4.0762

C. Electron impact excitation

Our calculated cross sections for electron impact excitation of CH_2^+ from the ground state to four of its lowest doublet states are shown in Figure 2. As in the elastic

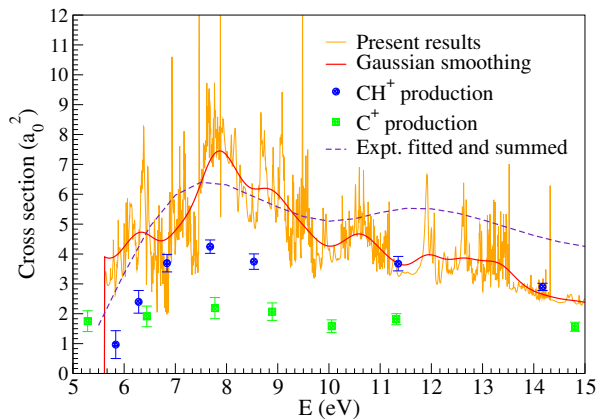


FIG. 3: Cross section for the electron impact dissociation of the CH_2^+ ion. Thin curve: present R-matrix results (see text). Thick (red) curve: present result after smoothing with a Gaussian function. Green circles with error bars: experimental results for C^+ ion production [12]. Blue circles with error bars: experimental results for CH^+ ion production [12]. Dashed curve: experimental results for C^+ and CH^+ ion production summed after suitable fitting (see text).

cross section, the excitation cross sections show highly resonant behaviour due to temporary captures into resonant states. Particularly, the $X^2A_1 \rightarrow 1^2B_1$ excitation cross section shows evidence of a large resonance near threshold. Referring to Figure 1, this is likely due to the large 3B_1 resonance near 1 eV as seen from the plot of the 3B_1 eigenphase sum. Generally, the excitation cross sections decrease with increasing incident energy and the cross sections from the higher lying excited states are much smaller.

D. Electron impact dissociation

Experimental cross sections for electron impact dissociation were obtained by [12] for the production of CH^+ and C^+ fragments. Although model calculations exist for the electron impact dissociation of CH_2^+ ions (see for example [2]), to the best of our knowledge, the 2007 experiments have never been described by any *ab initio* calculation.

The dissociation of CH_2^+ into the lowest dissociation channels, namely $e + \text{CH}^+ + \text{H}$ and $e + \text{C}^+ + \text{H}_2$, proceed via direct dissociative excitation and have thresholds 6.08 eV and 5.62 eV respectively [12]. In deriving the dissociation cross section, we assumed that electronic excitations to all states above the respective dissociation thresholds lead to dissociation. In our calculation, we have included the states 1^2B_1 , 1^2B_2 , 1^2A_2 , and the 2^2A_2 excited states all of which lie close to one another at the CH_2^+ equilibrium. Moreover, except the 1^2B_1 state, which has both valence and Rydberg character, all the other three are of valence character at equilibrium (see for example [18]) and hence are likely to dissociate to the $e + \text{C}^+ + \text{H}_2$ (5.62 eV) or the $e + \text{CH}^+ + \text{H}$ (6.08 eV) dissociation limits,

which are the most relevant in the energy range considered. Since the dissociation channels cannot be separated in our calculations, our cross section in Figure 3 represents a sum over these channels. For better comparison, we have also shown our cross sections after smoothing by using a Gaussian function. The experimental data from [12] are available for each of the dissociation channels mentioned above. The energy grid of the experimental cross sections for these two dissociation channels, however, are neither same nor uniform. Therefore, to sum the experimental data, we first spline interpolated each set over the same and uniform energy grid. This allowed us to sum the cross section for the experimental data. In Figure 3, this sum is shown as the dashed line and it agrees fairly well with our computed cross section. In particular, the peak near 8 eV agrees quite well with the spline interpolated summed experimental curve. However, we note that since the experimental data is non uniformly spaced, the interpolated curve may not often reflect the actual trend. For example, we suspect the agreement of the interpolated curve with our calculation would have been much better between 11 eV - 15 eV had there been more experimental points available in this region. Similarly, below 6 eV the interpolated experimental curve, appears to diverge for our Gaussian fitted curve. This is a result of the fitting procedure, the interpolated experimental curve actually follows the trend of our raw cross section curve.

IV. CONCLUSION

As mentioned in the introduction, CH_2^+ is a very important constituent in low temperature plasma environments. However, despite its importance, electron collisions studies on CH_2^+ have been rare. In fact, we could not find any *ab initio* calculation for the cross sections included in the present work. The only cross section result available, seems to be the total ionisation cross section of CH_2^+ calculated within the Binary-Encounter-Bethe (BEB) model by [44].

In this work, we have presented a reliable set of cross sections for the electronic excitation, and electron impact dissociation of the CH_2^+ ion. In fact, none of these cross sections have ever been reported before by any *ab initio* calculation. Additionally, we have also calculated and have given the position and width for some of the Feshbach resonances in the $e\text{-CH}_2^+$ system. These Feshbach resonances, as is well known, are the routes to dissociative recombination of the CH_2^+ ion. However, its treatment requires a more comprehensive calculation of the resonance energies, widths and the potential energy surfaces of the CH_2^+ states. This is the subject of an ongoing project.

Acknowledgements

The authors acknowledge support from Fédération de Recherche Fusion par Confinement Magnétique (CNRS, CEA and Eurofusion), La Région Normandie, FEDER

and LabEx EMC3 via the projects PTOLEMEE, Bioengine, the Institute for Energy, Propulsion and Environment (FR-IEPE), and ERASMUS-plus conventions between Université Le Havre Normandie and University College London. We are indebted to Agence Nationale de la Recherche (ANR) via the project MONA, Centre National de la Recherche Scientifique via the Programme National 'Physique et Chimie du Milieu Interstellaire' (PCMI). JZsM thanks the financial support of the National Research, Development and Innovation Fund of Hungary (NKFIH), under the K18 and FK19 funding

schemes with project no. K128621 and FK132989. JZsM and IFS are grateful for the support of the NKFIH-2019-2.1.11-TÉT-2020-00100 and Campus France-Programme Hubert Curien-BALATON-46909PM projects.

Data availability

Upon a reasonable request, the data supporting this article will be provided by the corresponding author.

-
- [1] McLean A G, Elder J D, Stangeby P C, Allen S L, Boedo J A, Brooks N H, Fenstermacher M E, Groth M, Lisgo S, Nagy A, Rudakov D L, Wampler W R, Watkins J G, West W P, and Whyte D G 2005 *J. Nucl. Materials* **337-339**, 124–128.
- [2] Reiter D and Janev R K 2010 *Contrib. Plasma Phys.* **50**, 986.
- [3] Janev R K and Reiter D 2002a *Phys. Plasmas* **9**, 4071.
- [4] Janev R K and Reiter D 2002b *Collision Processes of Hydrocarbon Species in Hydrogen Plasmas: I. The Methane Family* (Available from: Forschungszentrum-Jülich, Jülich, Germany).
- [5] Wakelam V, Smith I W M, Herbst E, Troe J, Geppert W, Linnartz H, K. Öberg, Roueff E, Agúndez M, Pernot P, Cuppen H M, Loison J C, and Talbi D 2010 *Space Sci. Rev.* **156**, 13.
- [6] Larson Å, Padellec A L, Semaniak J, Strömholm C, Larsson M, Roßen S, Peverall R, Danared H, Djuric N, Dunn G H, and Datz S 1998 *The Astrophysical Journal* **505**, 459.
- [7] IdBarkach T, Chabot M, Béroff K, Negra S D, Lesrel J, Geslin F, Padellec A L, Mahajan T, and Díaz-Tendero S 2019 *Astron. Astrophys.* **628**, A75.
- [8] Puglisi A, Miteva T, and J Paul Mosnier E T K, Bizau J M, Cubaynes D, Sisourat N, and Carniato S 2018 *Phys. Chem. Chem. Phys.* **20**, 4415.
- [9] van Dishoeck E F, Beaerda R A, and van Hemert M C 1996 *Astron. Astrophys.* **307**, 645.
- [10] van Dishoeck E F, Jonkheid E F, and van Hemert M C 2006 *Faraday Discuss.* **133**, 231.
- [11] Lecointre J, Belic D S, Jureta J J, Janev R K, and Defrance P 2009 *Euro. Phys. J D* **55**, 569.
- [12] Vane C R, Bahati E M, Bannister M E, and Thomas R D 2007 *Phys. Rev. A* **75**, 052715.
- [13] Guo L, Ma H, Zhang L, Song Y, and Li Y 2018 *Rsc. Adv.* **8**, 13635.
- [14] Ma H, Zhang C, Song Y, Ma F, and Li Y 2021 *J. Phys. Chem. A* **125**, 5490
- [15] Kraemer W P, Jensen P, and Bunker P R 1994 *Can. J. Phys.* **72**, 871.
- [16] Li Y Q, Zhang P Y, and Han K L 2015 *J. Chem. Phys.* **142**, 124302.
- [17] Tennyson J and Sutcliffe B T 1983 *J. Mol. Spectrosc.* **101**, 71.
- [18] Theodorakopoulos G and Petsalakis I D 1991 *J. Molec. Struct. (THEOCHEM)* **230**, 205.
- [19] Bunker P R, Chan M C, Kraemer W P and Jensen P 2001 *Chem. Phys. Lett.* **341**, 358.
- [20] Jensen P, Wesolowski S S, Brinkmann N R, Richardson N A, Yamaguchi Y, Schaefer H F, and Bunker P R 2002 *J. Mol. Spectrosc.* **211**, 254.
- [21] Rösslein M, Gabrys C M, Jagod K F, and Oka T 1992 *J. Mol. Spectrosc.* **153**, 738.
- [22] Wang H, Neese C F, Morong C P, Kleshcheva M, and Oka T 2013 *J. Phys. Chem.* **117**, 9908.
- [23] Willitsch S and Merkt F 2003 *J. Chem. Phys.* **118**, 2235.
- [24] Chakrabarti K, Dora A, Ghosh R, Choudhury B S, and Tennyson J 2017 *J. Phys. B: At. Mol. Opt. Phys.* **50**, 175202.
- [25] Chakrabarti K, Ghosh R, and Choudhury B S 2019 *J. Phys. B: At. Mol. Opt. Phys.* **52**, 105205.
- [26] Chakrabarti K, Mezei J Z, Motapon O, Faure A, Dulieu O, Hassouni K, and Schneider I F 2018 *J. Phys. B: At. Mol. Opt. Phys.* **51**, 104002.
- [27] Ghosh R, Chakrabarti K, and Choudhury B S 2020 *Plasma Sources Sci. Technol.* **29**, 095016.
- [28] Tennyson J 2010 *Phys. Rep.* **491**, 29–76.
- [29] Burke P G 2011 *R-Matrix Theory of Atomic Collisions* Springer-Verlag:Heidelberg.
- [30] Carr J M, Galiatsatos P G, Gorfinkiel J D, Harvey A G, Lysaght M A, Madden D, Mašín Z, Plummer M, Tennyson J, and Varambhia H N 2012 *Euro. Phys. J. D* **66**, 58.
- [31] Pritchard B P, Altarawy D, Didier B, Gibson T D, and Windus T L 2019 *J. Chem. Inf. Model.* **59**, 4814.
- [32] Graber T, Kanter E P, Vager Z, and Zajfman Z 1993 *J. Chem. Phys.* **98**, 7725.
- [33] Pople J A and Curtiss L A 1987 *J. Phys. Chem* **91**, 155.
- [34] Brinkmann N R, Richardson N A, Wesolowski S S, Yamaguchi Y, and Schaefer III H F 2002 *Chem. Phys. Lett.* **352**, 505.
- [35] Osmann G, Bunker P R, Kraemer W P and Jensen P 1999 *Chem. Phys. Lett.* **309**, 299.
- [36] Faure A, Gorfinkiel J D, Morgan L A, and Tennyson J 2002 *Comput. Phys. Commun.* **144**, 224.
- [37] Römelt J and Peyerimhoff D 1981 *Chem. Phys.* **54**, 147.
- [38] Yamaguchi Y and Schaefer III H F 1997 *J. Chem. Phys.* **106**, 1819.
- [39] Noble C J and Nesbet R K 1984 *Comput. Phys. Commun.* **33**, 399.
- [40] Zhang R, Baluja K L, Franz J, and Tennyson J 2011 *J. Phys. B: At. Mol. Opt. Phys.* **44**, 035203.
- [41] Sarpal B K, Branchett S E, Tennyson J, and Morgan L A 1991 *J. Phys. B: At. Mol. Opt. Phys.* **24**, 3685–99.
- [42] Rabadán I and Tennyson J 1996 *J. Phys. B: At. Mol. Opt. Phys.* **29**, 3747–61.
- [43] Tennyson J and Noble C J 1984 *Comput. Phys. Commun.* **33**, 421.
- [44] Irikura K K, Kim Y K, and Ali M A 2002 *J. Res. Natl. Inst. Stand. Technol.* **107**, 63.